Order and conformation of biphenyl in cyanobiphenyl liquid crystals. A combined atomistic molecular dynamics and ^{1}H-NMR study

Antonio Pizzirusso[†], Maria Enrica Di Pietro[‡], Giuseppina De Luca[‡],
Giorgio Celebre[‡*], Marcello Longeri[‡], Luca Muccioli[†], Claudio Zannoni[†*]

Abstract

We report an investigation of the alignment of biphenyl (2P) in the liquid crystal phases of 5CB and 8CB, combining predictive atomistic Molecular Dynamics (MD) simulations and ^{1}H-LXNMR residual dipolar couplings measurements. We provide first a detailed comparison and validation of the MD results with LXNMR, showing a good agreement between the simulated and experimental dipolar couplings at the same reduced temperature. We then use MD to examine the location of biphenyl in the smectic, by itself unavailable to LXNMR and find that, surprisingly, it is rather uniformly distributed. We show that the combination of MD and NMR provides very detailed information about the order, the interconnection between orientation and conformation, the local positional order and interactions with the liquid crystalline solvent.

1   Introduction

Various recent atomistic molecular dynamics (MD) simulation studies of liquid crystals (LC) have proved that this technique can now aim at reproducing actual experimental results, and provide "realistic" predictions for density,

---

[†]Dipartimento di Chimica Industriale "Toso Montanari", and INSTM, Università di Bologna, Viale Risorgimento 4, 40136 Bologna, Italy

[‡]Dipartimento di Chimica e Tecnologie Chimiche, Università della Calabria, Via P. Bucci, 87036 Arcavacata di Rende, Italy

[*]Corresponding authors: Giorgio.Celebre@unical.it, Claudio.Zannoni@unibo.it

transition temperatures, order parameters and other observables [1–11]. Of course, the success of this effort is strictly connected to the quality of the Force Field (FF), the set of intra and intermolecular interactions employed, which must inevitably be tested and/or parameterized versus experimental observations. Among the experimental techniques, Liquid Crystal NMR (LXNMR) spectroscopy [12] represents an invaluable test-bed for LC simulations, because the step between molecular and observable properties is much more rigorously defined than in other techniques (e.g. dielectric or birefrigence) where problems like internal field corrections or intermolecular correlations inevitably affect the analysis of the results.

Indeed some of the most important LXNMR observables, namely the residual nuclear dipolar coupling constants (RDCs) of a solute in a LC, obtained after the non-trivial assignment of its spectral lines [13], can be also expressed as averages of well defined functions of atomic coordinates and order parameters that can be calculated from the simulations. Unfortunately, while the couplings D_{IJ} between two protons I, J of a flexible solute can be extremely informative on its molecular geometry, conformation, and average orientation, the spectral analysis becomes increasingly complex because of the high number of lines resulting upon adding new coupled proton spins. For this type of analysis, atomistic simulations in conjunction with efficient algorithms for fitting the LXNMR spectra, like the one recently proposed by Meerts et al. [14] based on evolutionary optimization methods, promise to significantly increase the range of molecules amenable to be studied. The simulated dipolar couplings could in fact serve as a useful starting point for the spectral fitting algorithm in cases that would be otherwise impossible to solve in a reasonable time. A realistic simulation of the dipolar couplings can also provide insights on some still not completely clear fundamental mechanisms of the studied systems (as, for example, the nature of the dominant orientational interactions [15–21]) and a few attempts along this line have been recently published by some of us [6, 7, 22].

Beyond this important, but somehow technical aspect of helping in the spectral analysis and line assignment, an even more exciting possibility is that of combining MD and NMR to extend the range of properties that can be reliably investigated. For instance, while LXNMR excels at obtaining orientational properties, it cannot provide directly positional order, even if, given the importance of the problem, proposals to obtain indirectly positional information with the help of mean field [23, 24] or density functional theory [25, 26] have been put forward to this effect. Given the inevitable introduction of approximations in these approaches, an alternative possibility explored here is to validate atomistic MD by comparing in detail orientational properties with LXNMR results and then use MD to predict positional or-

der and other properties, e.g. correlation functions, not easily available from experiment. It is clear that both for exploiting in a systematic way the simulated D_{IJ} to help the experimental analysis and for testing the predictive capability of MD, the accuracy, in absolute terms, of the predicted couplings as well as their temperature dependence must be first investigated.

To this end, here we have tackled a joint experimental and MD simulated ^{1}H-LXNMR study of one of the most important and well studied flexible aromatic π-conjugated molecules, biphenyl (2P), employed as a solute in the liquid crystalline phases of 4-n-pentyl, 4$'$cyanobiphenyl (5CB) and 4-n-octyl, 4$'$cyanobiphenyl (8CB, figure 1), at different temperatures. The choice originates on one hand from the availability of a reliable force field for n-cyanobiphenyls [22, 27] and on the other from the abundant literature on the NMR spectra of biphenyl in several LC solvents [28–34], even if the case of biphenyl in n-alkylcyanobiphenyl liquid crystals has never been treated before neither theoretically nor experimentally. Since, despite its high symmetry and relatively small size, the biphenyl 10-spin system is close the limit of what can now be analyzed by conventional techniques [13], the prior knowledge is helpful in this exercise.
Besides being a building block for liquid crystalline compounds and semiconducting polymers, biphenyl is a classical example of a non-rigid molecule presenting the possibility of a strong coupling between internal conformation and environment [28, 34]. For instance 2P, like many oligoaromatic compounds, is twisted with an inter-ring angle of around 44 degrees in the gas phase [35], with various quantum chemistry methods giving values between 38 and 46 degrees [36], while on the contrary 2P is found to be flat in the crystal phase [37]. In nematic liquid crystal solvents instead, NMR experiments consistently indicate a preferred twist angle of around 35 degrees [28, 31–34]. It is then also interesting to investigate the coupling between the phenyl-phenyl dihedral angle, both in the solute and the solvents, and the alignment and biaxiality of the corresponding conformers, like we do in the second part of the article.

2   Materials and Methods

2.1   Preparation of the Samples, NMR Experiments and Analysis of ^{1}H-LXNMR Spectra

Two dilute solutions (2 wt% and 2.8 wt% respectively) were prepared by dissolving biphenyl in the liquid crystal solvents 5CB and 8CB (all compounds were purchased from Aldrich). As expected, by varying the temperature,

the first sample (2P/5CB) exhibited only a nematic phase while the second (2P/8CB), besides the nematic, showed also a double layer smectic A phase (referred to as smectic or simply S in the remainder of the article). More in detail, for the 2 wt% solution of 2P in 5CB (added of a 0.26 % of 1,3,5-trichlorobenzene (TCB) as a reference orientational probe, the transition temperatures recorded on cooling the sample from the isotropic phase were: T_{NI}=308 K and T_{KN}=291 K, while the literature transition temperatures for the pure 5CB are : T_{NI}=308.3 K and T_{KN}=297.3 K on cooling [38]. For the second sample, the 2.8 wt% solution of 2P in 8CB (also added of a 0.26 % of TCB) the transition temperatures recorded in a cooling scan were: T_{NI}=311 K; T_{SN}=303 K; $T_{KS} \ll$294.5 K (supercooling often occurs), while the transition temperatures reported for the pure 8CB are [39] T_{NI}=313.6 K; T_{SN}=306.6 K; T_{KS}=294.5 K.

For recording the spectra, the samples 2P/5CB and 2P/8CB were heated a few times up to their nematic-isotropic transition temperature, strongly shaken to homogenize the solutions, then left to cool slowly in the magnetic field of the NMR spectrometer. The proton spectra were recorded at different reduced temperatures $T_r \equiv T/T_{NI}$, thermostating for 40-50 min for each temperature. The working temperatures ranged from 283 K to 304 K for 2P/5CB (corresponding to a T_r range $0.92 - 0.99$) and from 273 K to 307 K for 2P/8CB (0.88-0.99 overall in terms of T_r, where the smectic phase is in the range 0.88-0.96). All the spectra were recorded on a Bruker Avance 500MHz (11.74 T) instrument, equipped with a Bruker BVT 2000 temperature control unit. The analysis of the spectra was carried out using the home-made iterative computer program ARCANA [40] and the resulting dipolar couplings between hydrogens pairs (see fig. 1 for the labelling) are reported in Supporting Information in table S2 for 2P/5CB and table S3 for 2P/8CB.

2.2   Computer Simulations

Solutions of 2P in the liquid crystal solvents 5CB and 8CB have been simulated by the MD technique at atomistic level. To compare with LXNMR results, the samples have been built to be as close as possible to the real experimental systems studied. The first system studied was composed of 1904 molecules of 5CB, 16 molecules ($\sim$ 0.6 %wt) of TCB and 80 molecules ($\sim$ 2.5 %wt) of 2P, while the second one consisted of 1892 8CB molecules, 8 molecules ($\sim$ 0.2 %wt) of TCB and 100 molecules ($\sim$ 2.7 %wt) of 2P. The biphenyl and TCB solutes have been described with full atomistic detail starting from the AMBER-OPLS force field [41]; their charge distributions have been computed with the quantum chemistry ESP method [42],

4

using the Gaussian09 code [43], the PBE0 density functional [44] and the cc-pVTZ basis set. The torsional potential for the phenyl-phenyl rotation of 2P has been calculated at the same level of theory. The solvent molecules have instead been modeled at united atoms (UA) level of detail, using a previously validated force field [22].

We have run NPT simulations with periodic boundary conditions, using the MD engine NAMD [45] with Berendsen thermostat and barostat [46], at the following thermodynamic conditions: P=1 atm, T=285 K, 290 K, 295 K, 300 K, 301 K, 302 K, 303 K and 305 K for 2P/5CB, and T=294 K, 296 K, 298 K, 300 K, 302 K, 304 K and 306 K for 2P/8CB. Electrostatic contributions have been evaluated with the Particle Mesh Ewald method [47] using a grid spacing of 1.2 Å for each box side; the scaling factors for 1–4 electrostatic and Lennard Jones intramolecular interactions were set to 5/6 and to 1/2 respectively [48]. We have employed a multiple time step method for integrating the equations of motion, where the bonding, Lennard -Jones and electrostatic interactions were calculated with a time step of 1, 2 and 4 fs respectively for a total MD production time of at least 50 ns at each temperature.

The force field parameters for the 2P phenyl-phenyl torsional potential deserve particular attention, as this can subtly influence the orientational order in the LC solvent and also affect the values of inter-ring dipolar couplings, as each conformation experiences, at least in principle, a different orienting field. Here we obtained the optimized structure at PBE0//cc-pVTZ level with Gaussian09 software [43]. We then proceeded to perform relaxed scans of the phenyl-phenyl torsional potential, generating a reference profile to be inserted in our molecular mechanics force field. This profile, shown in fig. S2, presents an equilibrium twist angle of ~ 39 degrees, in agreement with previous calculations [36, 49] performed for 2P in vacuum. The indirect contribution $U_c(\varphi)$ of the other terms of the FF to the effective torsional potential has been estimated as the potential of mean force acting at φ. This was in turn obtained from a separate MD simulation of an isolated molecule at T=300 K, in which the FF explicit torsional potential was fixed to zero, using the Adaptive Biasing Force (ABF) method [50, 51], that allows an easy calculation of the free energy profile for a given driving variable (in this case the dihedral angle φ). The difference between the DFT torsional potential and $U_c(\varphi)$ was then fitted with a truncated Fourier series which was employed as the new explicit FF torsional potential. To validate this procedure, we have checked the new effective potential first with a further ABF run, this time using the new FF parameters shown in table 1, then with a separate MD simulation at 300 K of a 2P molecules in a cubic box with sides of 50 Å surrounded by 25 Ar atoms to ensure proper thermal exchange. The corresponding effective

Table 1: Phenyl-phenyl torsional potential coefficients u_n in the truncated Fourier series $U(\varphi) = \sum_n u_n \cos(n\varphi)$: calculated at PBE0//cc-pVTZ level (VTZ) in vacuum; as implemented in the molecular mechanics force field after the removal of the indirect contribution (FF); in cyanobiphenyls as obtained from the analysis of NMR RDCs with the additive potential method [34] and by means of MD simulations. The units are kcal/mol.

u_n	Force Field		AP method			MD simulation		
	VTZ	FF	5CB	8CB-S	8CB-N	5CB	8CB-S	8CB-N
u_0	1.07	1.54	1.89	1.56	1.63	1.30	1.30	1.26
u_2	-0.44	-1.37	-1.80	-1.45	-1.49	-1.14	-1.13	-1.07
u_4	1.02	-0.12	1.99	1.66	1.74	1.06	1.08	1.07
u_6	0.18	-0.05	-0.19	-0.15	-0.16	0.13	0.10	0.11
u_8	0.06	-0.03	0.46	0.38	0.40	0.03	0.05	0.05
u_{10}	0.03	0.00	-0.06	-0.04	-0.05	0.03	0.02	0.03
u_{12}	0.01	0.00	0.12	0.10	0.11	0.01	0.01	0.01

torsional potential was then calculated through the inversion of the distribution $P(\varphi)$ of the dihedral angle: $U(\varphi) = -k_B T \ln P(\varphi)$, finding a good agreement between the two techniques (see Supporting Information fig. S2).

2.3 Simulated Observables

The orientational order for the liquid crystal solvent and for the solute are key quantities to be calculated. Here we have followed a procedure similar to that proposed in [6]. We start determining the instantaneous LC solvent director $\mathbf{n}(t_j)$ by setting up and diagonalizing the ordering matrix, $\mathbf{Q}$ for a sample configuration at time t_j:

$$\mathbf{Q}(t_j) = \sum_{i=1}^{N_{LC}} [3\mathbf{u}_i(t_j) \otimes \mathbf{u}_i(t_j) - \mathbf{I}]/(2N_{LC}) \tag{1}$$

where $\mathbf{u}_i$ is the chosen reference molecular axis of the i-th LC molecule ($i = 1, ...N_{LC}$), $\mathbf{I}$ is the identity matrix and LC is either 5CB or 8CB. The instantaneous solvent order parameter corresponds to the largest eigenvalue of $\mathbf{Q}(t_j)$, i.e. $\lambda^+(t_j)$ [22], while the corresponding eigenvector is the instantaneous director $\mathbf{n}(t_j)$. The average order of the solvent, $\langle P_2 \rangle_{LC}$ is then obtained as the time average over M equilibrated configurations:

$$\langle P_2 \rangle_{LC} = \frac{1}{M} \sum_j^M \lambda^+(t_j). \tag{2}$$

6

For determining the solute order parameter $\langle P_2 \rangle_S$ from the MD trajectories we used the instantaneous director $\mathbf{n}(t_j)$ for the configuration at time t_j for computing the angle β_i between the phase director and the reference axis $\mathbf{u}_i$ of the i-th molecule, and taking a sample average, followed by a time average:

$$\langle P_2 \rangle_S = \frac{1}{MN_S} \sum_j^M \sum_i^{N_S} \left\{ \frac{3}{2} [\, \mathbf{u}_i(t_j) \cdot \mathbf{n}(t_j)]^2 - \frac{1}{2} \right\}, \tag{3}$$

where the index i runs over all the N_S molecules of a given species in a configuration and j on all the M configurations constituting the production trajectory. The reference axis for 2P, 5CB and 8CB is chosen here as the principal axis for the inertia tensor of the molecule at time t_j, i.e. the eigenvector corresponding to its lowest eigenvalue. From the simulated trajectories we can also determine the residual dipolar couplings:

$$D_{IJ} = -\frac{\mu_0}{8\pi^2} \gamma_I \gamma_J \hbar \left\langle \frac{P_2(\hat{\mathbf{r}}_{IJ} \cdot \mathbf{n})}{r_{IJ}^3} \right\rangle \tag{4}$$

where $\mathbf{r}_{IJ} = r_{IJ} \hat{\mathbf{r}}_{IJ}$ is the vector connecting two nuclei I and J at distance r_{IJ}, $\mu_0 = 4\pi \cdot 10^{-7} \mathrm{T}^2 \mathrm{J}^{-1} \mathrm{m}^3$ is the magnetic permeability in vacuum; $\gamma_I = g_I \mu_N / \hbar$ is the nuclear gyromagnetic ratio of nucleus I. In general the angular brackets indicate here averaging over any relevant molecular motion (namely, the small-amplitude high-frequency vibrations, the internal torsions and the overall reorientational motions, e.g. that of the long axis also known as "molecular tumbling" or that around the long axis, called "spinning"). The standard deviations for the simulated D_{IJ} have been estimated with the blocking method described by Flyvbjerg and Petersen [52].

Once $\mathbf{n}(t_j)$ is known, the instantaneous angles between $\mathbf{n}(t_j)$ and the axes of a cartesian, molecule fixed coordinate system $(\mathbf{u}_x, \mathbf{u}_y, \mathbf{u}_z)$ can be used to calculate the components of the instantaneous symmetric and traceless Saupe order tensor [53]:

$$S_{ab}(t_j) = 3\langle [\mathbf{n}(t_j) \cdot \mathbf{u}_a][\mathbf{n}(t_j) \cdot \mathbf{u}_b] - \delta_{ab} \rangle / 2 \tag{5}$$

where a, b are the indexes of the three axis of the molecular frame and δ_{ab} is the Kronecker delta function. The observable Saupe ordering matrix S_{ab} is calculated as a time average of $S_{ab}(t_j)$. Here, like in reference [34], we computed the average values of S_{ab} for 2P, 5CB and 8CB as a function of the phenyl-phenyl dihedral angle φ choosing a molecular frame where $\mathbf{u}_z$ is parallel to the biphenyl long axis and $\mathbf{u}_x$ is normal to $\mathbf{u}_z$ while bisecting the angle φ. Hence for $\varphi = 0$, the biphenyl unit is planar and $\mathbf{u}_x$ lies on the molecular plane and $\mathbf{u}_y$ is normal to it.
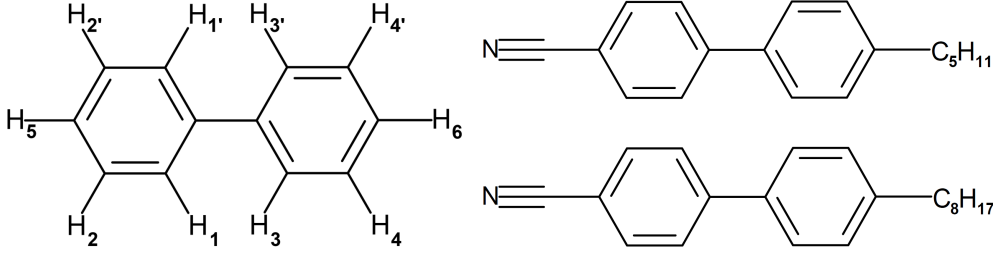
Figure 1: Chemical structure of the solute biphenyl with labelling of its hydrogens (left), and of the liquid crystalline solvents 5CB and 8CB (right).

While the single particle observables suffice to make a comparison with LX-NMR, MD can provide useful information also on two particle properties and in particular on spatial pair correlations. To characterize the positional order in the smectic phase of 8CB we employed the center of mass-center of mass radial distribution along the phase director:

$$g(z_{12}) \quad = \quad \frac{1}{\pi R^2 \rho} \langle \delta(z_{ik} - z_{12}) \rangle \tag{6}$$

where z_{ik} is the projection of the intermolecular vector $\mathbf{r}_{ik}$ between molecules i and k along the director $\mathbf{n}$, ρ is the number density, and R is the radius of the cylindrical sampling region (in our case, about 70 Å, see ref. [27] for details). The correlation between two molecules is also expected to be anisotropic and to vary when their separation vector $\mathbf{r}_{ik}$ is at different angles β_{ik} with respect to the director. This can be examined with the anisotropic radial distribution function, $g(r_{12}, \cos \beta_{12})$:

$$g(r_{12}, \cos \beta_{12}) \quad = \quad \frac{1}{4\pi r^2 \rho} \langle \delta(r_{ik} - r_{12}) \delta(\cos \beta_{ik} - \cos \beta_{r_{12}}) \rangle \tag{7}$$

that we calculate and plot in the last section.

3   Results and discussions

3.1   Phase behaviour and orientational order

The very first comparison between LC simulations and experiments can be drawn on the basis of the measured transition temperatures. Although this could seem a rather simple task, it is worth noting that even reproducing with computer simulations the experimental liquid crystal phases is still far from being a straightforward achievement [54]. On one hand obtaining the correct phase sequence is difficult as the difference in free energy between

8

LC phases or the corresponding transition enthalpies are often close to the accuracy that can be obtained with empirical force fields (about 1 kcal/mol). Moreover, even in the correct phase behaviour is achieved, the transition temperatures can still be subjected to very large shifts (even 100 K) with respect to the experimental values [9,55–58]. The best accuracy obtained at the moment, after specific optimization of the FF is of the order of 1-4 K for the nematic-isotropic transition temperature T_{NI} of 5CB [59], 8CB [22] and the nematic-smectic transition temperature of 8CB [27]. A further complication that arises when studying a mixture is that, even though the pure components may be well described by the adopted force field, the mixed interactions may not be as satisfactory. The issue is particulary delicate for the case of a solute dissolved in a LC phase, which typically has the effect of a partial disruption of the orientational order, translating into a destabilization of the nematic phase, and in a consequent shift of the nematic–isotropic transition to lower temperatures [60]. In our case even the small concentrations used are sufficient to produce shifts of up to 2-3 K on the $N-I$ and $S-N$ phase transition temperatures with respect to the pure solvents. Thus the order of magnitude of the shift is comparable to the error expected in the simulation transition temperatures. The phase organizations and their transition temperatures are thus the first result to look for when simulating liquid crystalline systems, in our case the 2P/5CB and 2P/8CB solutions. Starting with phase organizations, a simple visual inspection of the equilibrated solvent arrangement in the simulated samples confirms that the two LC solvents are respectively in their nematic and smectic phases at room temperature (figure 2). This is gratifying, as experimentally the range of existence of the smectic phase in the 2P/8CB solution is quite limited (around 8 K as we have seen in the previous section) We take this as a first confirmation of the validity of our force field, already verified for the pure cyanobiphenyl solvents and for dilute solutions of several small rigid molecules [6, 7] and of pentane [7] dissolved in 5CB, also for the present case.

The most sensible way of comparing measurements of orientational order-dependent properties in different LC solvents and concentrations or, as in our case, experiment with simulations is to refer to the same reduced temperature $T_r = T/T_{NI}$ instead of the absolute one [7, 60, 61]. It becomes then important to estimate the nematic-isotropic transition temperature as accurately as possible also with simulations. To this end, once approximately individuated the temperature range where the T_{NI} occurs, we have performed additional simulations in a narrow temperature range encompassing the phase transition, and assigned the T_{NI} by inspecting the distribution of the instantaneous configuration order parameter $P_2(t)$ both for the solvents [22] and the solute at those temperatures, as shown in figure 3. In all cases we selected the in-

9

lowest

(highest)

termediate value between the highest temperature at which the distribution is centered at $P_2 \simeq 0.3$ (shown in light blue) and the lowest temperature possessing a distribution centered around $P_2 \simeq 0.1$ (light red). With this criterion the transition temperatures obtained are 302.5±0.5 K for 2P/5CB (≈2.5 wt%) and 305±1 K for 2P/8CB (≈2.7 wt%). Interestingly both the distributions of the order parameter of the solvents and those for the solute produce the same estimated values, a first indication that the order of the phase is correctly transferred to biphenyl. In addition, in both solutions the expected downshift of the T_{NI} upon solute insertion is qualitatively reproduced. However the consequences of doping with a small quantity of biphenyl appear to be somewhat overestimated, with a decrease of T_{NI} of 4-6 K versus the experimental observation of 1-2 K. In other words, with respect to reality, the simulations describe a situation where the doping of the solvent compromises in a more significant way the ordering of the system we are studying. However, by plotting the experimental and simulated results of the average nematic order parameter $\langle P_2 \rangle$ versus temperature (figure 4) it emerges that apart the small differences in transition temperatures, the two curves have very similar slopes and the values of the order parameters themselves also match very well. In figure 4 we mark with dashed black vertical lines not only the nematic-isotropic transition temperature for 5CB and 8CB, but also the smectic-nematic transition temperature, estimated to occur at about 301 K from the sinusoidal trend of the pair distribution function along the director $g(z_{12})$ (vide infra, reference [27] and Supporting Information). In the same figure we report also the order parameter of 2P predicted from simulations as a function of temperature: we see that it does follow the solvent one, but also that it is significantly lower. The experimental values for 2P were instead calculated by assuming the molecule to be rigid and using the simulation geometry [62]. Since with MD we measured a nearly perfect proportionality between $\langle P \rangle_{LC}$ and $\langle P \rangle_{2P}$, with a proportionality factor of 0.645 (figure S1), we used it for calculating a pseudo experimental order parameter also for 5CB and 8CB [62]. MD seems to systematically underestimate the experiment when the order is plotted against temperature, and conversely to produce slightly larger values when the data are plotted against the reduced temperature (figure 4, bottom plates); despite these small deviations, the simulated order parameter is always very similar to the experimental one.
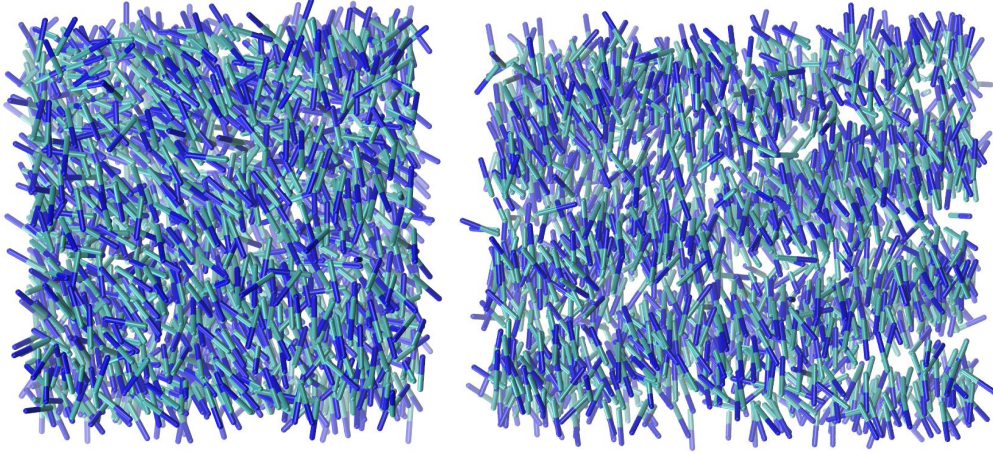
10

Figure 2: Snapshots of the liquid crystal solvent for the two samples equilibrated at 300 K. 5CB (left) appears to be in the nematic phase while for the 8CB sample, beside the orientational order, a layered structure can be visually detected (right). Molecules are represented as rods joining the cyano nitrogen with the 4′ phenyl carbon.
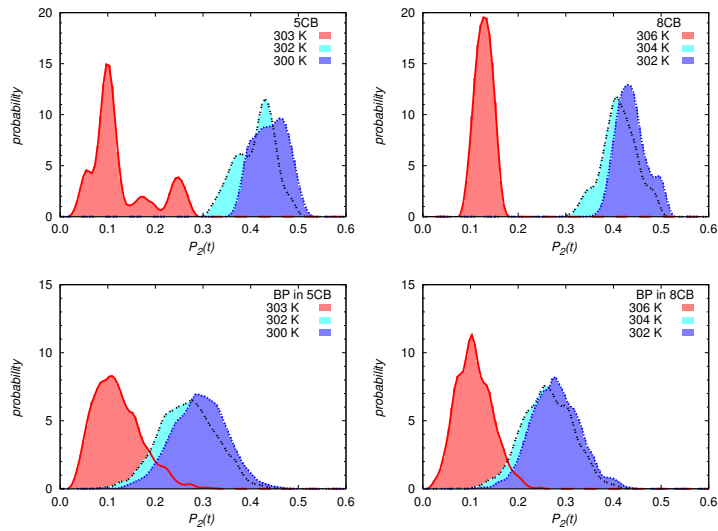

Figure 3: Distribution functions of the nematic order parameter P_2 for LC solvents (top) and biphenyl solute (bottom). The distributions at higher temperature (red) correspond to the isotropic liquid phase, while the cyan and blue histograms correspond to nematic phase temperatures.
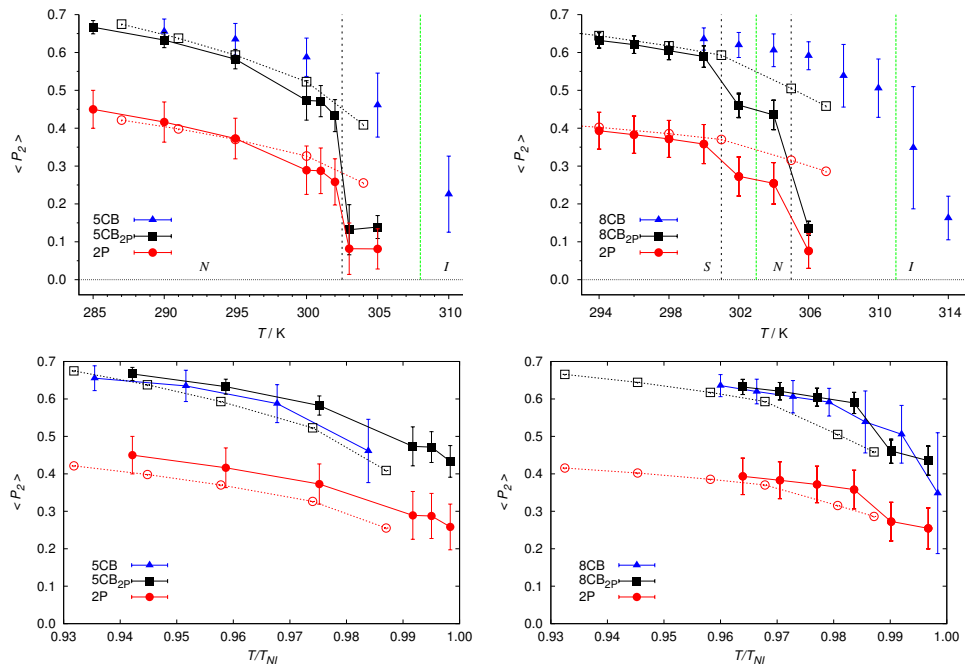
11

Figure 4: Top plates: order parameters of cyanobiphenyls (black) and 2P (red) obtained by MD simulations (filled symbols) and experiments (empty symbols [62]) as a function of temperature. The simulated transition temperatures for 2P/5CB (left) and 2P/8CB (right) are indicated by dashed vertical black lines, while experimental ones are drawn in green. Simulation data for pure 5CB and 8CB (blue points) are taken from references [22, 27]. Bottom plates: the same quantities plotted against the reduced temperature. Solid lines are a guide to the eye.

3.2 Comparison between experimental and simulated dipolar couplings

Once assessed the similarity between experimental and simulated phase diagrams and assigned the phase transition temperatures, we proceeded to a thorough analysis of biphenyl ^{1}H residual dipolar couplings. Owing to the high symmetry of the 2P molecule, its ten protons give rise to only twelve independent couplings (see figure 1 and table 2), which nevertheless are sufficient to produce complex NMR spectra. These are quite laborious to analyze without the help of sophisticated algorithms [7], though in this specific case the abundant prior knowledge [28, 32, 34, 63] simplifies the task. Even easier is the calculation of observable dipolar couplings for a pair of nuclei from the MD simulation trajectories, where they are given by simple analytical formulae once assumed the phase director to be at a well defined angle (for cyanobiphenyls just coincident) with the magnetic field direction [12, 53, 64]. For our sample sizes and simulation lengths (about 100 solute molecules and 100 ns), the standard deviations on the calculated RDCs are of the order of 1-10 Hz and typically lower than 1%, hence the statistics seems adequate for the comparison with the NMR experiment. As already mentioned, it would be convenient to employ the simulated couplings as a first guess in either manual or automatic assignment procedures of the experimental ones, but as we aim at testing the reliability of simulated RDCs, here we compare all the 2P couplings obtained independently with the two methods. It must be stressed that this comparison is much more severe than simply comparing the typically large order parameter of the long axis for a solute or solvent, because many RDCs are also affected by the conformation of the molecule, and their orientation may be very different from the one of the phase director, sometimes being close to the so-called magic angle, at which $P_2(\mathbf{r}_{ij} \cdot \mathbf{n})$ and $D_{ij} = 0$ also in presence of orientational order. To provide a quick visual comparison, our predictions for the RDCs of 2P in 5CB and 8CB are plotted in figures 5 and 6 together with the experimental values and against T_r, while in table 2 we report the explicit values for a few reduced temperatures. In general, the couplings present very similar but not identical values, with differences within a few tenths of Hz for the small couplings, or with percentage deviations of about 10% for the largest coupling D_{12}, D_{13}, D_{14}. These differences can be explained in terms of a slight overestimation of the alignment of the long axis of 2P in the simulations at a given reduced temperature, as clearly shown by the graphs of D_{12} and D_{16} in figures 5 and 6. It is also worth noting that all the signs of the couplings are correct, and that the simulation prediction is marginally better for 8CB than for 5CB, in particular in the smectic phase. There exists, however, a specific coupling, D_{25},

13

for which the agreement with experiment is not satisfactory, with differences of the order of 100 Hz or 300%. The particularity of this coupling resides in the short distance between the protons involved, which magnifies the absolute error, while the relative one can be already very large as the orientation of the vector is close to the magic angle (MD indicates an order parameter $P_2^{25} \approx 0.02$, see also Supporting Information). Only the combination of the two effects in the numerator and denominator of Equation 4 seem to produce this high uncertainty: for instance D_{12}, that has a short interproton distance but high P_2, and $D_{12'}$ that conversely is generated by two protons relatively far away from each other but with an average orientation very close to the magic angle, are both satisfactorily reproduced by MD simulations.

A final discussion element emerging from inspecting figures 5 and 6 is that the slopes of the simulated and real curves match very well, independently on the nature of the coupling, as also D_{25} and the inter-ring, conformational-dependent couplings D_{13} and D_{14} all exhibit the correct behavior. This important result could possibly be exploited for aiding the multi-temperature analysis of experimental data. Clearly, if the quality of the simulation predictions we report here is representative of the current computational capabilities, any automated method using these couplings as input must be flexible enough to tolerate an initial guess with values sometimes rather different from the real ones.

Table 2: Experimental and simulated RDCs (Hz) for biphenyl at a few selected reduced temperatures, corresponding to the nematic phase of 5CB and to the nematic and smectic phase of 8CB.

| D_{ij}	5CB NMR $T_r = 0.974$	5CB MD $T_r = 0.975$	8CB NMR $T_r = 0.987$	8CB MD $T_r = 0.990$	8CB NMR $T_r = 0.968$	8CB MD $T_r = 0.970$
D_{12}	-2658.03 ± 0.04	-3008 ± 12	-2348.86 ± 0.08	-2205 ± 23	-3022.42 ± 0.03	-3094 ± 13
$D_{12'}$	-3.22 ± 0.06	-17 ± 1	-6.77 ± 0.11	-17 ± 1	-5.05 ± 0.04	-16 ± 1
D_{13}	-890.02 ± 0.09	-866 ± 16	-771.09 ± 0.16	-623 ± 10	-1004.91 ± 0.06	-895 ± 8
$D_{11'}$	158.89 ± 0.15	148 ± 2	132.39 ± 0.28	99 ± 3	177.16 ± 0.10	156 ± 2
$D_{22'}$	158.05 ± 0.15	149 ± 2	131.69 ± 0.28	99 ± 3	176.90 ± 0.11	157 ± 2
D_{14}	-226.42 ± 0.05	-257 ± 1	-200.64 ± 0.08	-189 ± 1	-257.51 ± 0.03	-264 ± 1
D_{15}	-336.38 ± 0.11	-386 ± 2	-298.88 ± 0.22	-285 ± 3	-383.78 ± 0.09	-396 ± 2
D_{16}	-156.48 ± 0.11	-180 ± 1	-139.88 ± 0.23	-133 ± 1	-178.78 ± 0.08	-185 ± 1
D_{24}	-84.10 ± 0.12	-96.8 ± 0.5	-75.47 ± 0.17	-71 ± 1	-96.17 ± 0.07	-99.4 ± 0.4
D_{25}	-35.15 ± 0.13	-150 ± 8	-62.23 ± 0.21	-149 ± 6	-51.75 ± 0.08	-139 ± 6
D_{26}	-64.32 ± 0.13	-73.6 ± 0.3	-56.39 ± 0.22	-54 ± 1	-73.25 ± 0.08	-75.7 ± 0.3
D_{56}	-50.93 ± 0.06	-57.9 ± 0.5	-44.66 ± 0.14	-43 ± 1	-57.76 ± 0.05	-60 ± 1
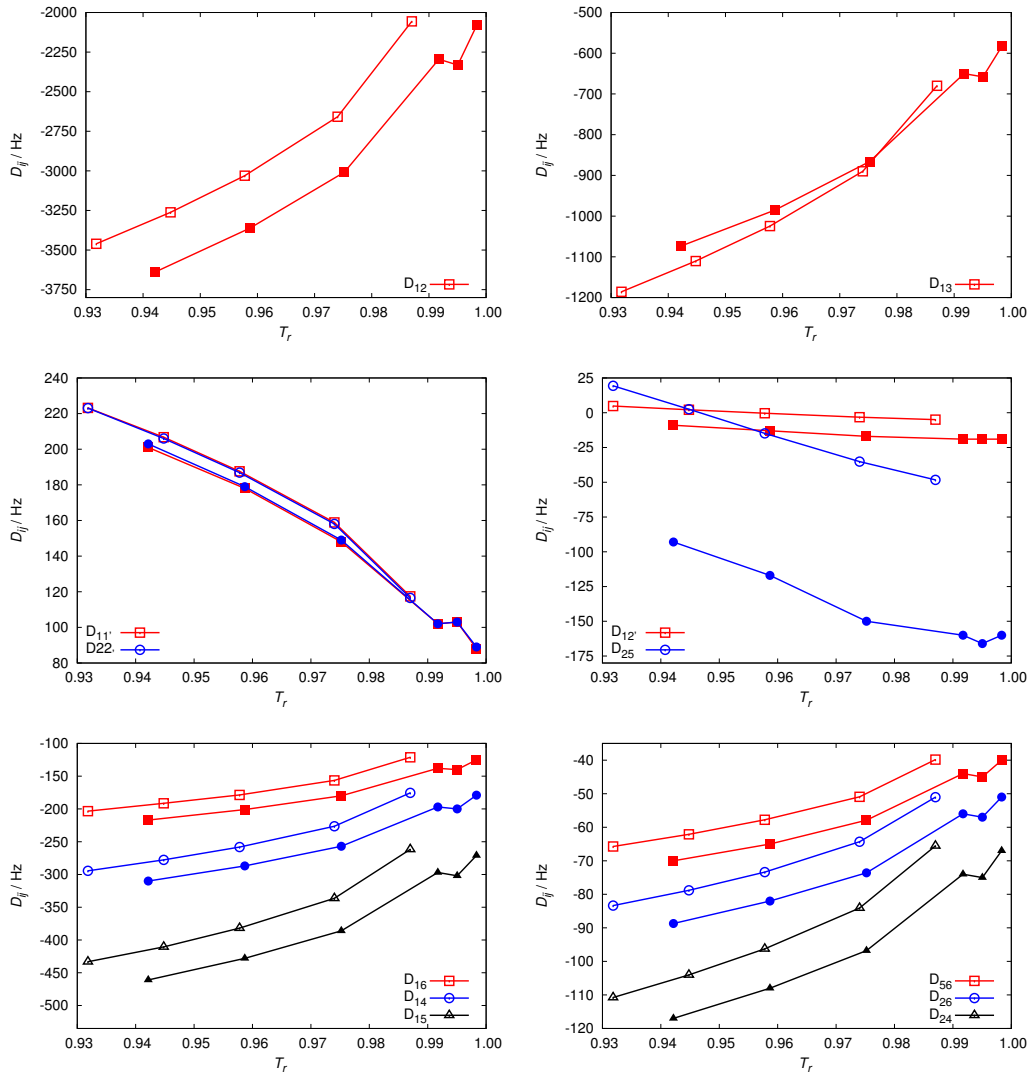
Figure 5: Comparison of experimental (empty symbols) and simulated (filled symbols) dipolar couplings as function of $T_r = T/T_{NI}$ for 2P/5CB system. Solid lines are a guide to the eye.
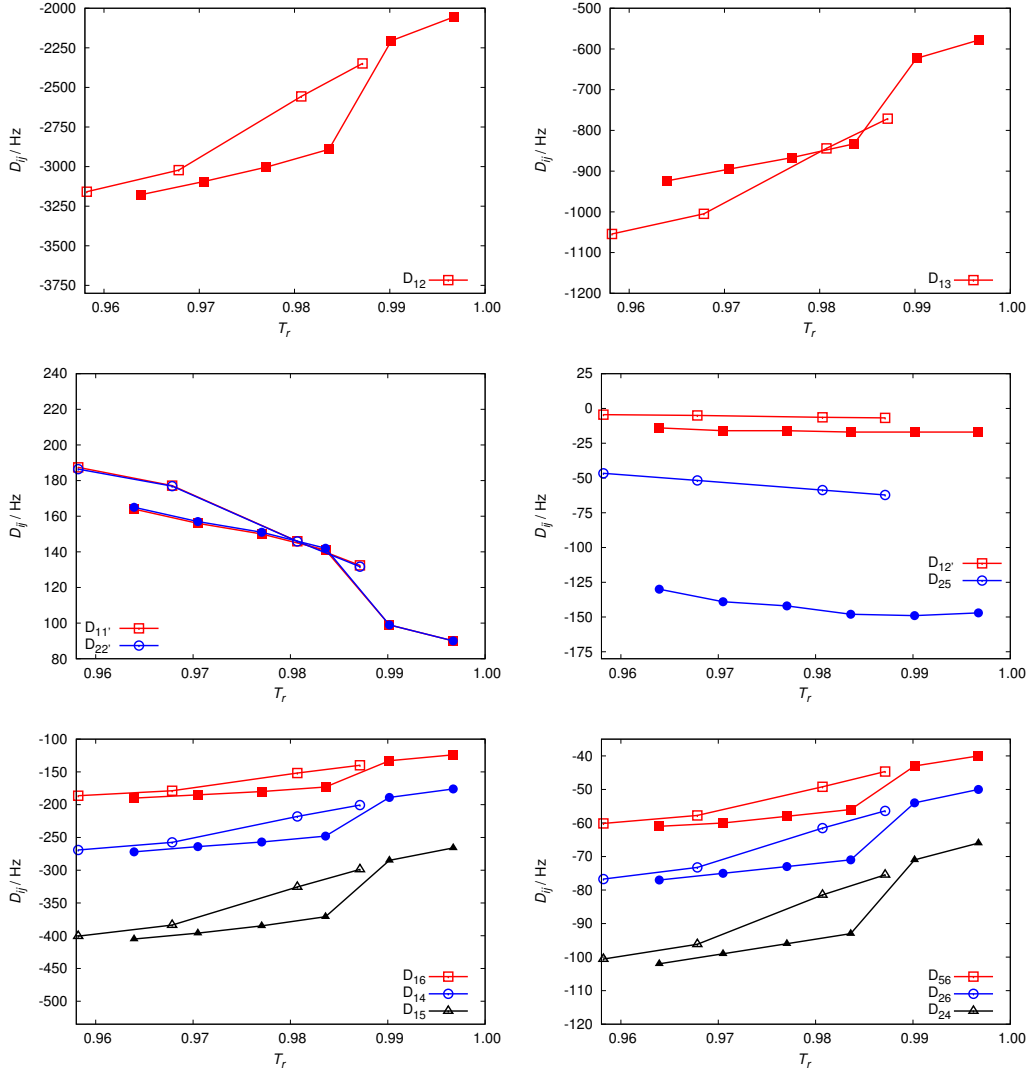
15

Figure 6: Comparison of experimental (empty symbols) and simulated (filled symbols) dipolar couplings as function of T_r in 2P/8CB system. Appreciable jumps are visible in correspondence of both the experimental and simulated the Smectic-Nematic transition. Solid lines are a guide to the eye.

3.3 Conformation and orientation

The feasibility of internal rotation of biphenyl makes its conformation in principle sensitive to the local solvation environment. In turn, as conformers differ in shape, when surrounded by an orientationally ordered medium they may experience a different interaction strength and hence possess dissimilar values of their alignment tensor [31, 33, 34]. To understand the effect of the anisotropic solvation environment on conformation, we start by comparing the probability distributions obtained from MD simulations in 5CB and 8CB with the same calculated here analysing the experimental dipolar couplings via the Additive Potential-Direct Probability Distribution method(AP-DPD). For for a general description and application examples of the AP philosophy, see e. g. references [65] and [66] ; for the teoretical foundations of the AP-DPD method, see [34] and references therein. Figure 7 shows that the profiles for 2P in 5CB and 8CB are very similar and in particular the positions of the maxima of conformational probability all fall between 34 and 35 degrees. We also notice, when comparing the inter-ring torsion distribution of biphenyl in 5CB and in 8CB with the "gas phase" one, obtained from the QM-DFT torsional energy profile, that a shift of about 4-5 degrees of the "equilibrium" angle towards more flat phenyl-phenyl conformations is induced by the LC solvent.

To further investigate the extent of the coupling between the orientational order of the solvent and the conformation of the solute, we investigated the dependence on of the Saupe matrix elements for the long (S_{zz}) and short biphenyl axis (S_{xx}) and of its biaxiality $S_{xx} - S_{yy}$ on the phenyl-phenyl angle φ. These quantities are shown in figure 8 for biphenyl dissolved in 5CB and 8CB at different temperatures, and compared with the corresponding ones obtained by analyzing the experimental RDCs with the variant of the additive potential method described in reference [34]. Qualitatively the two sets of data are very similar, with the main differences arising from the previously discussed temperature shift with temperature of T_{NI} and of the order parameter $\langle P_2 \rangle$ values shown in figure 4. A strong similarity is shared also by the behavior in the two solvents 5CB and 8CB: in particular even the change of phase from nematic to smectic of the latter (the two lower temperatures in figure 8) does not seem to alter the strength of the conformation-orientation coupling with respect to 5CB. Overall we find a very weak influence of the conformation on the alignment of the long axis of 2P with MD and NMR, suggesting variations lower than 10% (note that for our choice of molecular axes, S_{zz} coincides with P_2). Surprisingly enough, for both methods the conformation of maximum alignment is not the most biaxial and planar at $\varphi=0°$, but the much more uniaxial and twisted ones ($\varphi \approx 60°$ for MD and $\varphi \approx 90°$
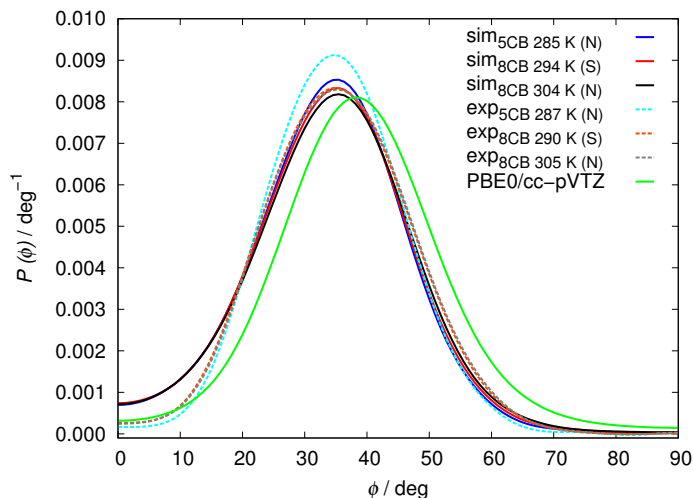
Figure 7: Distribution of phenyl-phenyl torsion angle in LC calculated with the AP method (cyan, orange and gray dashed lines) and MD simulation (blue, red and black filled lines), as function of the studied temperatures. The calculated Boltzmann distribution in gas phase for biphenyl at 300 K using the PBE0//cc-pVTZ potential (green line) is also reported. The raw simulation data were symmetrized and smoothed by fitting them with a series of cosines like the one used in table 1.

for NMR). The biaxiality of alignment $S_{xx} - S_{yy}$ is indeed strongly coupled with conformation, and it assumes rather high positive values (0.1-0.25) for all dihedral angles lower than 60 degrees.

With respect to ^{1}H-NMR, simulations present the advantage of being able to provide access to the order of the solvent with the same (virtual) experiment: therefore we calculated the Saupe matrix diagonal elements also for 5CB and 8CB, as shown in figure 9 as a function of the phenyl-phenyl torsion angle θ (the biphenyl unit is present in these compounds as well, as we see from figure 1). Even for the case of the solvent order tensor, the differences between 5CB and 8CB are minimal, and the maximum values for S_{zz} fall at twisted geometries, but unlike the case of the solute, the biaxiality of the orientation with respect to the phase director is very weak, and more generally the coupling between biphenyl conformation and orientation can be considered negligible - indisputably an effect of the presence of the uniaxial cyano unit and of the flexible alkyl chains.
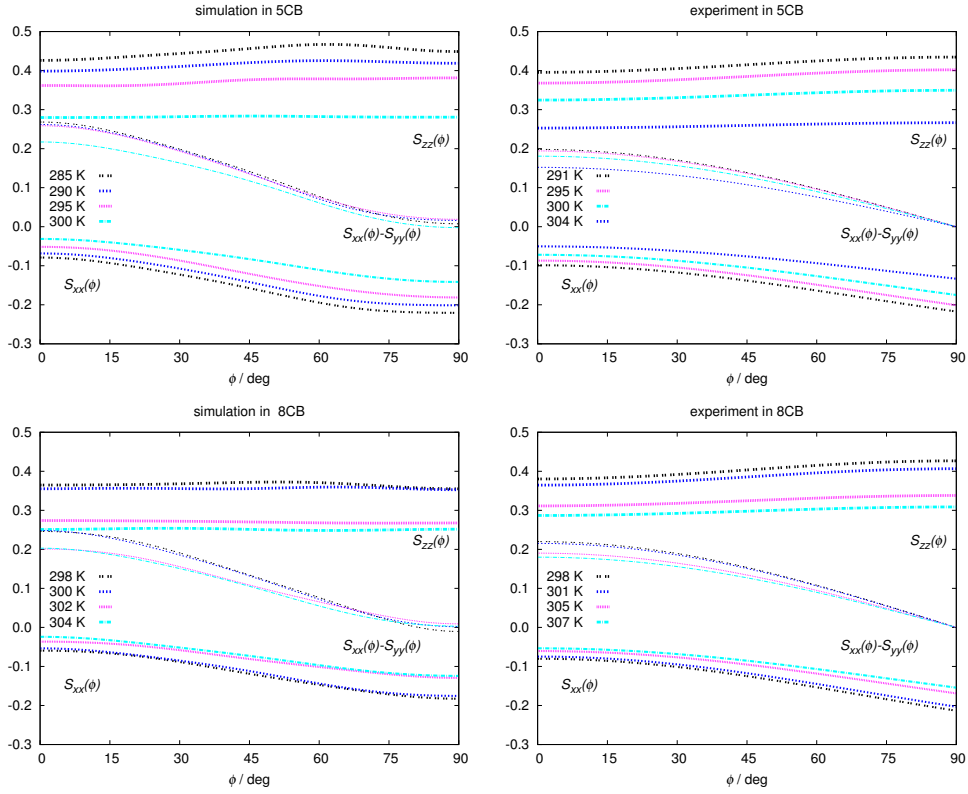
Figure 8: Dependence of Saupe matrix diagonal elements on the value of 2P phenyl-phenyl dihedral angle, as obtained from MD simulations (left panels) and from AP analysis of experimental data(right panels) in 2P/5CB (top) and 2P/8CB mixtures (bottom). The raw simulation data were symmetrized and smoothed by fitting them with a series of cosines like the one used in table 1.
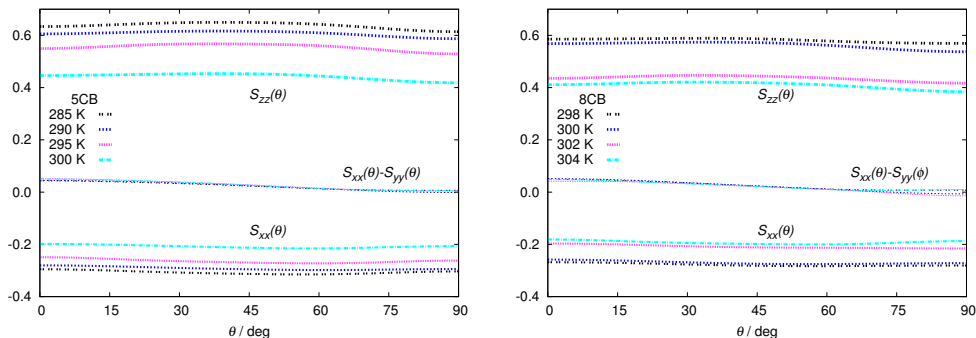
19

Figure 9: Simulated dependence of Saupe matrix diagonal elements on the value of 2P phenyl-phenyl dihedral angle for 5CB (left) and 8CB solvents (right). The raw simulation data were symmetrized and smoothed by fitting them with a series of cosines like the one used in table 1.

3.4 Positional order of biphenyl

The results discussed so far concerning the orientational order of the solute suggest little or no differences at all when switching the solvent from 5CB to 8CB, despite that the second compound also exhibits a smectic phase, instead of just a nematic. The smectic phase of 8CB consists in strongly interdigitated bilayers formed by two polar layers of molecules featuring an antiparallel arrangement of the molecular dipoles [27]. The solute then could inherit the positional order of the phase, in particular considering the expected affinity of biphenyl for the corresponding chemical groups present in 8CB, that are partially microsegregated in the layered structure. The standard computational observable for monitoring the positional order along a given direction is the normalized two particle correlation function $g(z_{12})$, which gives the distribution of the intermolecular distance $\mathbf{r}_{12}$ projected along the director of the LC phase ($z_{12} = \mathbf{r}_{12} \cdot \hat{n}$) [27]. In the presence of layers along the chosen direction, this function displays oscillations with a period corresponding to the layer spacing d, while it remains flat otherwise. As expected on the basis of our previous simulation results on pure 8CB [27] and from inspecting the snapshot in figure 2, below 302 K the solvent $g(z_{12})$ for the 2P/8CB solution shows periodic undulations spaced of about 31 Å, a value in close agreement with the experimental values for the pure mesogen [67] (see figure 10 and supporting information). Conversely, we found no evidence of spatial correlation, neither between 2P molecules, nor between biphenyl and 8CB, whose rather noisy $g(z_{12})$ distribution in the phase does not have any regular undulation. This very flat positional distribution function measured for biphenyl in 8CB, suggests that 2P cannot be an effective probe for the
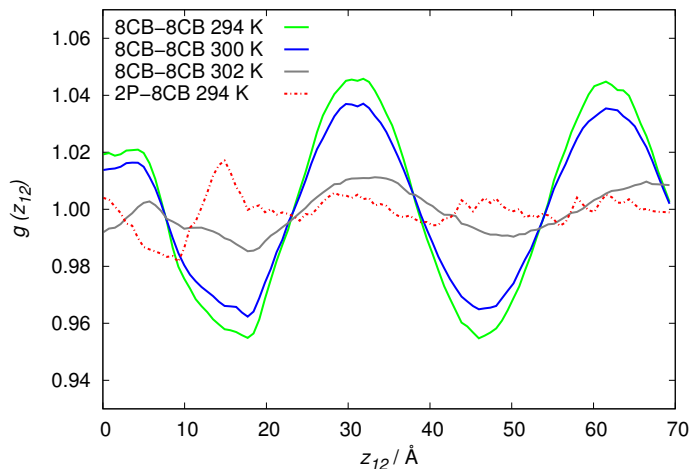
20

Figure 10: Two particle correlation function of the intermolecular distance along the alignment direction z of 8CB showing the existence of layers in the smectic phase (T=294 and 300 K), and only a weak spatial correlation in the nematic phase (302 K). The corresponding mixed correlation function between 8CB and 2P is also shown.

positional order parameter of the phase it is dissolved in, differently from what was recently shown, by a combination of NMR and theory, for some rigid solutes in the LC 4,4′ di-n-heptyl-azoxybenzene [25, 68] and 4-cyano-4′ -n-octyloxybiphenyl [26].

The absence of long–range positional order for 2P does not exclude the possibility of short range intermolecular correlations. To further investigate this aspect, we calculated the radial distribution of the solvent-solute intermolecular distance as a function of the orientation of the corresponding vector with respect to the phase director. The two-dimensional maps plotted in figure 11 provide a further confirmation that for the biphenyl solute the 5CB and 8CB solvents are almost indistinguishable, independently on the nature of their LC phase. In all the plots, only one intense peak appears at 4-6 Å and $\cos \beta_{12} < 0.5$, corresponding to 2P molecules facing the biphenyl group of 8CB ones aligned with the director ("face to face"). Weak replica of this peak appear at about 9.5 and 14 Å, indicating 8CB/2P pairs with the same arrangement but separated by one or two interposed 8CB molecules. The second peak in terms of intensity arises instead by pairs of molecules in a "head to tail" arrangement, always with the 8CB aligned with the director, giving an intermolecular distance of about 15.5 Å but at $\cos \beta_{12} \approx 1$.
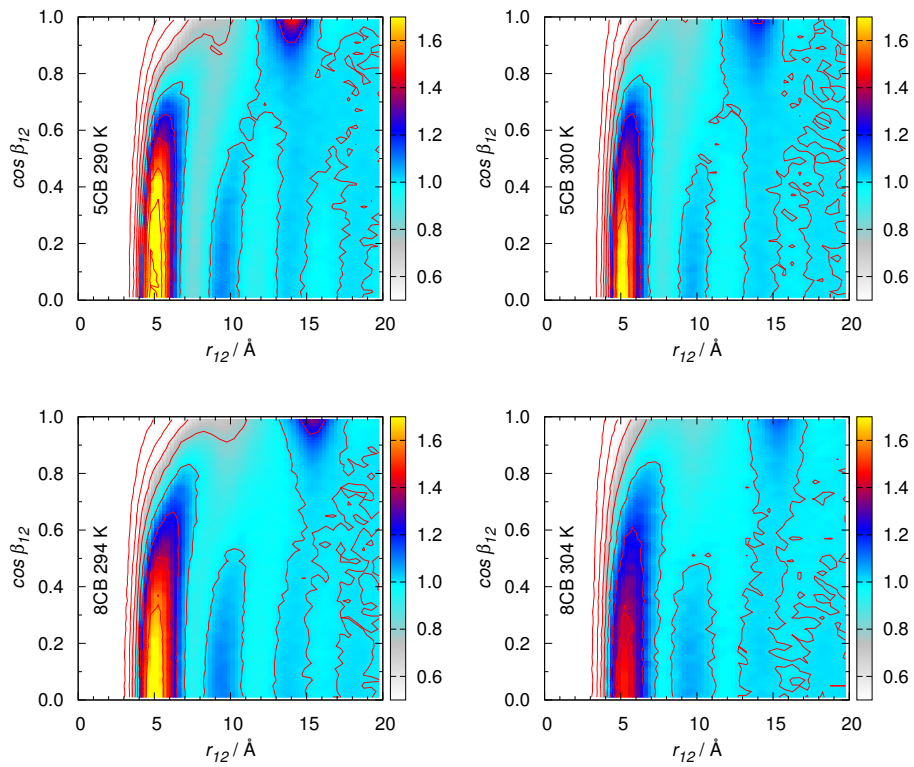
Figure 11: Mixed radial-orientational distribution function of the solvent-solute center of mass intermolecular distance r_{12} as a function of its orientation with the phase director $\cos \beta_{12} = \mathbf{r}_{12} \cdot \mathbf{n}$. Top: results at two temperatures of the 5CB nematic phase, bottom: smectic (left) and nematic phase of 8CB (right).

4   Conclusions

The order and conformation of the non rigid biphenyl solute in 5CB and 8CB liquid crystalline solutions has been studied in detail, examining the data obtained by experimental ^{1}H-NMR measurements and MD atomistic simulations. In a first part of the work we have validated the predictive capability of the MD simulations comparing orientational properties. We have shown that, once corrected for small shifts in the solvent transition temperatures by employing reduced temperatures, the simulated orientational order parameters and the residual dipolar couplings are in good agreement with the experimental ones, with typical differences in magnitude of a few tenths of Hz for small couplings and of about 10% for the large ones. Interestingly, the agreement is even better for the derivative of the couplings with respect to temperature, and we suggest to exploit also these simulation observables in future multi-temperature, computer-aided analysis of experimental data. MD and NMR produced very similar results also for the interplay between solute orientational order and conformation. Actually the alignment of the biphenyl long axis is only weakly coupled with the phenyl-phenyl torsion angle, but surprisingly, the coupling is stronger for uniaxial conformers with angles greater than 45 degrees. The orientational order of the two short axes is instead strongly conformation-dependent, and biaxial for flat conformers with angles lower than 45 degrees.

In the second part of the study we have employed this validated MD to determine the biphenyl positional order and some relevant molecular pair correlations in the smectic phase of 8CB. We did not find evidences of long range positional correlations, neither among biphenyl molecules nor between them and the solvent. Actually the interaction of biphenyl with 5CB and 8CB is very similar, irrespective of the LC phase being nematic or smectic: the extent of spatial correlation between cyanobiphenyls LC solvents and the 2P solute is only local, not extending further than 15-20 Å, i.e. the length of a solvent molecule.

We believe that the combination of atomistic molecular dynamics simulations and LXNMR shown above can provide a powerful tool to synergistically enhance the possibilities of reliably investigating solutes in liquid crystals beyond what can be obtained by the two separate techniques.
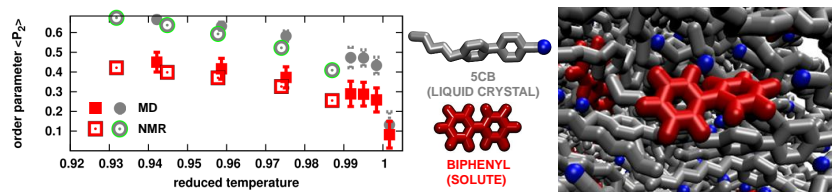
5   Acknowledgment

6 Keywords

Computer simulations, solute, nematic, smectic, residual dipolar couplings analysis.

7 TOC

A happy marriage of ^{1}H-NMR experiments and MD atomistic simulations validates the computer model and extends the range of information that can be gained on flexible solutes in liquid crystals.

References

[1] R. Berardi, L. Muccioli, C. Zannoni, *ChemPhysChem* **2004**, *5*, 104–111.

[2] J. Peláez, M. R. Wilson, *Phys. Rev. Lett.* **2006**, *97*, 267801.

[3] L. De Gaetani, G. Prampolini, *Soft Matter* **2009**, *5*, 3517–3526.

[4] A. Pizzirusso, M. Savini, L. Muccioli, C. Zannoni, *J. Mat. Chem.* **2011**, *21*, 125-133.

[5] J. G. Zhang, J. Y. Su, H. X. Guo, *J. Phys. Chem. B* **2011**, *115*, 2214-2227.

[6] A. Pizzirusso, M. B. D. Cicco, G. Tiberio, L. Muccioli, R. Berardi, C. Zannoni, *J. Phys. Chem. B* **2012**, *116*, 3760-3771.

[7] A. C. J. Weber, A. Pizzirusso, L. Muccioli, C. Zannoni, W. L. Meerts, C. A. de Lange, E. E. Burnell, *J. Chem. Phys.* **2012**, *136*, 174506.

[8] A. Pizzirusso, R. Berardi, L. Muccioli, M. Ricci, C. Zannoni, *Chem. Sci.* **2012**, *3*, 573-579.

[9] F. Chami, M. R. Wilson, V. S. Oganesyan, *Soft Matter* **2012**, *8*, 6823-6833.

[10] O. M. Roscioni, L. Muccioli, R. G. Della Valle, A. Pizzirusso, M. Ricci, C. Zannoni, *Langmuir* **2013**, *29*, 8950-8958.

[11] D. Täuber, C. von Borczyskowski, *Int. J. Mol. Sci.* **2013**, *14*, 19506–19525.

[12] E. E. Burnell, C. A. de Lange (eds.), *NMR of Ordered Liquids*, Kluwer, 2003.

[13] G. Celebre, G. De Luca, M. E. Di Pietro, *J. Phys. Chem. B* **2012**, *116*, 2876-2885.

[14] W. L. Meerts, C. A. de Lange, A. Weber, E. E. Burnell, *J. Chem. Phys.* **2009**, *130*, 044504.

[15] G. Celebre, *J. Chem. Phys.* **2001**, *115*, 9552-9556.

[16] G. Celebre, *Chem. Phys. Lett.* **2001**, *342*, 375-381.

[17] G. Celebre, G. De Luca, *Chem. Phys. Lett.* **2003**, *368*, 359-364.

[18] G. Celebre, G. De Luca, *J. Phys. Chem. B* **2003**, *107*, 3243-3250.

[19] G. Celebre, A. Ionescu, *J. Chem. Phys. B* **2010**, *114*, 228-234.

[20] G. Celebre, A. Ionescu, *J. Phys. Chem. B* **2010**, *114*, 235-241.

[21] G. Celebre, G. De Luca, M. Longeri, *eMagRes* **2013**, pp. 335–350.

[22] G. Tiberio, L. Muccioli, R. Berardi, C. Zannoni, *ChemPhysChem* **2009**, *10*, 125-136.

[23] A. Yethiraj, A. Weber, R. Y. Dong, E. E. Burnell, *J. Phys. Chem. B* **2007**, *111*, 1632–1639.

[24] E. E. Burnell, R. Y. Dong, A. C. J. Weber, X. Yang, A. Yethiraj, *Can. J. Chem.* **2011**, *89*, 900–908.

[25] M. E. Di Pietro, G. Celebre, G. De Luca, G. Cinacchi, *Phys. Rev. E* **2011**, *84*, 061703.

[26] M. E. Di Pietro, G. Celebre, G. De Luca, H. Zimmermann, G. Cinacchi, *Eur. Phys. J. E* **2012**, *35*, 1-10.

[27] M. F. Palermo, A. Pizzirusso, L. Muccioli, C. Zannoni, *J. Chem. Phys.* **2013**, *138*, 204901.

[28] G. Celebre, G. De Luca, M. Longeri, D. Catalano, C. A. Veracini, J. Emsley, *J. Chem. Soc. Faraday Trans.* **1991**, *87*, 2623-2627.

[29] D. Catalano, L. Di Bari, C. A. Veracini, G. N. Shilstone, C. Zannoni, *J. Chem. Phys.* **1991**, *94*, 3928-3935.

[30] T. Chandrakumar, J. M. Polson, E. E. Burnell, *J. Magn. Reson. A* **1996**, *118*, 264-271.

[31] R. Berardi, F. Spinozzi, C. Zannoni, *Mol. Cryst. Liq. Cryst.* **1996**, *290*, 245-253.

[32] G. Celebre, G. De Luca, G. Mazzone, *THEOCHEM* **2005**, *728*, 209-214.

[33] A. B. Sahakyan, A. G. Shahkhatuni, A. A. Shahkhatuni, H. A. Panosyan, *Magn. Reson. Chem.* **2008**, *46*, 144-149.

[34] G. Celebre, G. De Luca, M. Longeri, *Liq. Cryst.* **2010**, *37*, 923-933.

[35] A. Almenningen, O. Bastiansen, L. Fernholt, B. N. Cyvin, S. J. Cyvin, S. Samdal, *J. Mol. Struct.* **1985**, *128*, 59-76.

[36] M. P. Johansson, J. Olsen, *J. Chem. Theory Comput.* **2008**, *4*, 1460-1471.

[37] G.-P. Charbonneau, Y. Delugeard, *Acta Cryst.* **1976**, *B32*, 1420-1423.

[38] M. Hird, in *Physical Properties of Liquid Crystals: Nematics*, (eds. D. A. Dunmur, A. Fukuda, G. R. Luckhurst), INSPEC, IEE, 2001 pp. 3–16.

[39] A. Würflinger, M. Sandmann, in *Physical Properties of Liquid Crystals: Nematics*, (eds. D. A. Dunmur, A. Fukuda, G. R. Luckhurst), INSPEC, IEE, 2001 pp. 151–161.

[40] G. Celebre, G. De Luca, M. Longeri, E. Sicilia, *J. Chem. Inf. Comput. Sci.* **1994**, *37*, 539-545.

[41] W. L. Jorgensen, D. S. Maxwell, J. Tirado-Rives, *J. Am. Chem. Soc.* **1996**, *118*, 11225-11236.

[42] B. H. Besler, K. M. Merz Jr., P. A. Kollman, *J. Comput. Chem.* **1990**, *11*, 431-439.

[43] M. J. Frisch, *et al.*, *Gaussian 09, Revision A.1*, Gaussian, Inc., Wallingford, CT, 2009.

[44] C. Adamo, V. Barone, *J. Chem. Phys.* **1999**, *110*, 6158-6170.

[45] J. C. Phillips, R. Braun, W. Wang, J. Gumbart, E. Tajkhorshid, E. Villa, C. Chipot, R. D. Skeel, L. Kale, K. Schulten, *J. Comput. Chem.* **2005**, *26*, 1781-1802.

[46] H. J. C. Berendsen, J. P. M. Postma, W. F. van Gunsteren, A. Di Nola, J. R. Haak, *J. Chem. Phys.* **1984**, *81*, 3684-3690.

[47] U. Essmann, L. Perera, M. L. Berkowitz, T. A. Darden, H. Lee, L. G. Pedersen, *J. Chem. Phys.* **1995**, *103*, 8577-8593.

[48] W. D. Cornell, P. Cieplak, C. I. Bayly, I. R. Gould, K. M. Merz, D. M. Ferguson, D. C. Spellmeyer, T. Fox, J. W. Caldwell, P. A. Kollman, *J. Am. Chem. Soc.* **1995**, *117*, 5179-5197.

[49] I. Cacelli, G. Prampolini, *J. Chem. Phys. A.* **2003**, *107*, 8665-8670.

[50] E. Darvé, A. Pohorille, *J. Chem. Phys.* **2001**, *115*, 9169-9183.

[51] J. Hénin, C. Chipot, *J. Chem. Phys.* **2004**, *121*, 2904-2914.

[52] H. Flyvbjerg, H. G. Petersen, *J. Chem. Phys.* **1989**, *91*, 461-466.

[53] J. W. Emsley, J. C. Lindon, *NMR Spectroscopy using Liquid Crystal Solvents*, Pergamon Press, 1975.

[54] M. R. Wilson, *Chem. Soc. Rev.* **2007**, *36*, 1881-1888.

[55] A. J. McDonald, S. Hanna, *J. Chem. Phys.* **2006**, *124*, 164906.

[56] F. Yan, D. J. Earl, *Soft Matter* **2011**, *7*, 10266-10273.

[57] F. Yan, D. J. Earl, *J. Chem. Phys.* **2012**, *136*, 124506.

[58] B. Mukherjee, L. Delle Site, K. Kremer, C. Peter, *J. Phys. Chem. B* **2012**, *116*, 8474-8484.

[59] L. De Gaetani, G. Prampolini, A. Tani, *J. Phys. Chem. B* **2006**, *110*, 2847-2854.

[60] A. S. Taggar, C. J. Campbell, A. Yethiraj, E. E. Burnell, *J. Phys. Chem. B* **2006**, *110*, 1363-1368.

[61] R. T. Syvitski, M. Y. M. Pau, E. E. Burnell, *Chem. Phys.* **2002**, *117*, 376-384.

[62] Using equation 4, the experimental coupling D_{56}, the MD average $\langle r_{56} \rangle_{MD} = 9.17$ Å and assuming the 2P molecule to be rigid ($\langle P_2/r_{ij}^3 \rangle \approx \langle P_2 \rangle / \langle r \rangle^3$), we obtained $\langle P_2 \rangle_{2P}^{exp} = 8\pi^2 D_{56} \langle r_{56} \rangle_{MD}^3 / (\gamma_i \gamma_j \hbar \mu_0)$. Then we employed the least square fitting line $\langle P_2 \rangle_{2P}^{MD} = a \langle P_2 \rangle_{LC}^{MD}$ to estimate $\langle P_2 \rangle_{LC}^{exp}$ as $\langle P_2 \rangle_{2P}^{exp}/a$, with a=0.645 (see also Supporting Information).

[63] W. E. Palke, D. Catalano, G. Celebre, J. W. Emsley, *J. Chem. Phys.* **1996**, *105*, 7096-7033.

[64] J. Emsley (Ed.), *Nuclear Magnetic Resonance of Liquid Crystals*, Reidel, 1985.

[65] J. W. Emsley, G. R. Luckhurst, C. P. Stockley, *Proc. R. Soc. A* **1982**, *381*, 117-138.

[66] J. W. Emsley, G. De Luca, G. Celebre, M. Longeri, *Liq. Cryst.* **1996**, *20*, 569-575.

[67] N. Kapernaum, F. Giesselmann, *Phys. Rev. E* **2008**, *78*, 062701.

[68] G. Celebre, G. Cinacchi, G. De Luca, *J. Chem. Phys.* **2008**, *129*, 094509.

[69] L. De Gaetani, G. Prampolini, A. Tani, *J. Phys. Chem. B* **2007**, *111*, 7473-7477.

Supporting Information

Table S1: Structure and electrostatic properties of 2P calculated at BPE0//cc-pVTZ level. Dipole and traceless quadrupole moments are reported in the principal inertial frame.
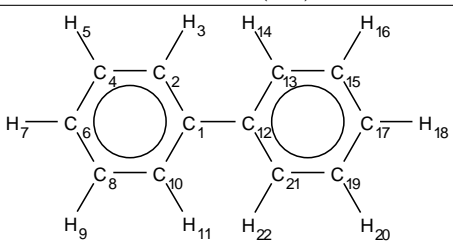
biphenyl (2P)		cc-pVTZ charges (e)			
		C1	+.07390	C12	+.07390
		C2	-.14590	C21	-.14590
		H3	+.11695	H22	+.11695
		C4	-.13230	C13	-.14590
		H5	+.12595	H14	+.11695
		C6	-.12590	C15	-.13230
		H7	+.12260	H16	+.12595
Dipole moment (Debye)		C8	-.13230	C17	-.12590
X=0.0 Y=0.0 Z=0.0		H9	+.12595	H18	+.12260
Quadrupole moment (Debye Å)		C10	-.14590	C19	-.13230
XX= 4.8 YY= 3.3 ZZ= -8.1		H11	+.11695	H20	+.12595

Table S2: Observed H-H dipolar couplings and chemical shift differences for biphenyl in 5CB at different temperatures (Hz). For the hydrogen labeling, see figure 1 in the main text.

	T = 283 K ($T_r = 0.92$)	T = 287 K ($T_r = 0.94$)	T = 291 K ($T_r = 0.95$)	T = 295 K ($T_r = 0.96$)	T = 300 K ($T_r = 0.98$)	T = 304 K ($T_r = 0.99$)
D_{12}	-3638.27 ± 0.07	-3460.42±0.06	-3261.84±0.04	-3030.39±0.04	-2658.03±0.04	-2055.70±0.06
D_{13}	-1254.87 ± 0.10	-1185.78±0.15	-1110.31±0.10	-1024.50±0.11	-890.02 ± 0.09	-679.96 ± 0.14
$D_{11'}$	239.76 ± 0.26	223.18 ± 0.21	206.74 ± 0.16	187.58 ± 0.13	158.89 ± 0.15	117.41 ± 0.19
$D_{22'}$	238.89 ± 0.22	223.06 ± 0.21	206.04 ± 0.10	186.85 ± 0.15	158.05 ± 0.15	116.51 ± 0.22
D_{14}	-309.72 ± 0.08	-294.40 ± 0.07	-277.69 ± 0.05	-258.17 ± 0.05	-226.42 ± 0.05	-175.50 ± 0.07
D_{24}	-116.57 ± 0.20	-110.77 ± 0.20	-104.04 ± 0.12	-96.26 ± 0.13	-84.10 ± 0.12	-65.55 ± 0.16
$D_{12'}$	7.22 ± 0.09	4.82 ± 0.08	2.14 ± 0.06	-0.38 ± 0.06	-3.22 ± 0.06	-4.99 ± 0.09
D_{16}	-213.91 ± 0.19	-203.38 ± 0.16	-191.41 ± 0.11	-178.65 ± 0.10	-156.48 ± 0.11	-121.25 ± 0.16
D_{15}	-455.09 ± 0.19	-433.19 ± 0.18	-410.58 ± 0.12	-381.92 ± 0.11	-336.38 ± 0.11	-261.72 ± 0.17
D_{26}	-89.54 ± 0.22	-83.36 ± 0.17	-78.80 ± 0.12	-73.37 ± 0.11	-64.32 ± 0.13	-51.04 ± 0.19
D_{25}	40.44 ± 0.23	19.36 ± 0.18	2.52 ± 0.13	-14.84 ± 0.11	-35.15 ± 0.13	-48.32 ± 0.17
D_{56}	-68.21 ± 0.14	-65.74 ± 0.10	-62.12 ± 0.08	-57.77 ± 0.06	-50.93 ± 0.06	-39.84 ± 0.10
$(\nu_1 - \nu_2)$	-511.09 ± 0.17	-471.81 ± 0.12	-442.80 ± 0.11	-401.27± 0.10	-339.39 ± 0.11	-232.66 ± 0.15
$(\nu_2 - \nu_5)$	-441.42 ± 0.19	-408.06 ± 0.12	-391.94 ± 0.12	-359.94 ± 0.10	-311.85 ± 0.11	-233.27 ± 0.16

Table S3: Observed H-H dipolar couplings and chemical shift differences for biphenyl in 8CB at different temperatures (Hz). For the hydrogen labeling, see figure 1 in the main text.

	T = 273 K ($T_r = 0.88$)	T = 277 K ($T_r = 0.89$)	T = 282 K ($T_r = 0.91$)	T = 286 K ($T_r = 0.92$)	T = 290 K ($T_r = 0.93$)
D_{12}	-3766.82 ± 0.05	-3686.11 ± 0.04	-3565.24 ± 0.05	-3481.88 ± 0.05	-3391.12 ± 0.03
D_{13}	-1284.43 ± 0.10	-1252.34 ± 0.08	-1205.94 ± 0.09	-1174.29 ± 0.11	-1140.11 ± 0.07
$D_{11'}$	236.76 ± 0.15	229.61 ± 0.13	218.99 ± 0.15	212.47 ± 0.17	205.33 ± 0.12
$D_{22'}$	235.85 ± 0.15	229.37 ± 0.12	218.66 ± 0.14	212.03 ± 0.17	204.32 ± 0.11
D_{14}	-317.02 ± 0.05	-313.98 ± 0.04	-303.63 ± 0.05	-300.79 ± 0.05	-289.01 ± 0.03
D_{24}	-119.63 ± 0.10	-117.27 ± 0.08	-113.54 ± 0.09	-110.33 ± 0.11	-107.82 ± 0.06
$D_{12'}$	1.55 ± 0.07	0.30 ± 0.05	-1.07 ± 0.06	-2.06 ± 0.06	-2.56 ± 0.05
D_{16}	-222.26 ± 0.12	-217.02 ± 0.11	-210.28 ± 0.12	-205.12 ± 0.16	-200.03 ± 0.09
D_{15}	-473.00 ± 0.12	-464.04 ± 0.10	-449.47 ± 0.13	-439.59 ± 0.15	-428.38 ± 0.09
D_{26}	-90.35 ± 0.12	-88.93 ± 0.10	-86.03 ± 0.12	-83.19 ± 0.16	-81.89 ± 0.09
D_{25}	-2.22 ± 0.12	-9.93 ± 0.10	-21.27 ± 0.12	-31.28 ± 0.15	-34.48 ± 0.09
D_{56}	-71.74 ± 0.09	-70.33 ± 0.07	-67.84 ± 0.08	-66.33 ± 0.09	-64.82 ± 0.06
$(\nu_1\text{-}\nu_2)$	-523.78 ± 0.12	-510.04 ± 0.09	-488.30 ± 0.12	-475.99 ± 0.13	-457.27 ± 0.09
$(\nu_2\text{-}\nu_5)$	-456.59 ± 0.12	-446.12 ± 0.10	-430.75 ± 0.12	-415.41 ± 0.13	-402.64 ± 0.09
	T=294 K ($T_r = 0.94$)	T = 298 K ($T_r = 0.96$)	T = 301 K ($T_r = 0.97$)	T = 305 K ($T_r = 0.98$)	T = 307 K ($T_r = 0.99$)
D_{12}	-3290.35 ± 0.03	-3158.86 ± 0.03	-3022.42 ± 0.03	-2556.68 ± 0.05	-2348.86 ± 0.08
D_{13}	-1102.17 ± 0.06	-1054.30 ± 0.06	-1004.91 ± 0.06	-844.09 ± 0.11	-771.09 ± 0.16
$D_{11'}$	196.66 ± 0.10	187.44 ± 0.10	177.16 ± 0.10	145.95 ± 0.17	132.39 ± 0.28
$D_{22'}$	197.51 ± 0.10	186.44 ± 0.10	176.90 ± 0.11	145.85 ± 0.17	131.69 ± 0.28
D_{14}	-280.65 ± 0.03	-269.17 ± 0.03	-257.51 ± 0.03	-217.93 ± 0.05	-200.64 ± 0.08
D_{24}	-105.08 ± 0.06	-100.57 ± 0.06	-96.17 ± 0.07	-81.45 ± 0.11	-75.47 ± 0.17
$D_{12'}$	-3.57 ± 0.04	-4.47 ± 0.04	-5.05 ± 0.04	-6.37 ± 0.07	-6.77 ± 0.11
D_{16}	-193.89 ± 0.08	-186.30 ± 0.09	-178.78 ± 0.08	-151.70 ± 0.14	-139.88 ± 0.23
D_{15}	-417.12 ± 0.08	-400.61 ± 0.09	-383.78 ± 0.09	-325.68 ± 0.14	-298.88 ± 0.22
D_{26}	-79.84 ± 0.08	-76.72 ± 0.09	-73.25 ± 0.08	-61.52 ± 0.13	-56.39 ± 0.22
D_{25}	-39.89 ± 0.08	-46.66 ± 0.08	-51.75 ± 0.08	-58.70 ± 0.13	-62.23 ± 0.21
D_{56}	-62.76 ± 0.06	-60.14 ± 0.05	-57.76 ± 0.05	-49.21 ± 0.09	-44.66 ± 0.14
$(\nu_1\text{-}\nu_2)$	-439.32 ± 0.12	-417.18 ± 0.08	-396.05 ± 0.10	-313.76 ± 0.08	-280.86 ± 0.20
$(\nu_2\text{-}\nu_5)$	-389.11 ± 0.08	-371.01 ± 0.08	-352.53 ± 0.08	-291.76 ± 0.14	-267.49 ± 0.20

Table S4: Simulated H-H solute dipolar couplings of selected hydrogen pairs (in Hz) for the case 2P/5CB. The ratios $\langle r_{ij}^{-3}\rangle/\langle r_{ij}\rangle^{-3}$ calculated from the simulations are given in square brackets. For the hydrogen labeling, see figure 1 in the main text.

	T = 285 K ($T_r = 0.942$)	T = 290 K ($T_r = 0.959$)	T = 295 K ($T_r = 0.975$)	T = 300 K ($T_r = 0.992$)	T = 301 K ($T_r = 0.995$)	T = 302 K ($T_r = 0.998$)
D_{12}	-3638 ± 16 [1.007]	-3362 ± 25 [1.007]	-3008 ± 12 [1.007]	-2295 ± 28 [1.007]	-2332 ± 24 [1.007]	-2082 ± 40 [1.007]
D_{13}	-1074 ± 11 [1.934]	-985 ± 14 [1.931]	-866 ± 16 [1.927]	-650 ± 10 [1.922]	-658 ± 8 [1.921]	-583 ± 16 [1.921]
$D_{11'}$	201 ± 3 [1.001]	178 ± 3 [1.001]	148 ± 2 [1.001]	102 ± 2 [1.001]	103 ± 3 [1.001]	88 ± 3 [1.001]
$D_{22'}$	203 ± 3 [1.001]	179 ± 3 [1.001]	149 ± 2 [1.001]	102 ± 2 [1.001]	103 ± 3 [1.001]	89 ± 3 [1.001]
D_{14}	-310 ± 1 [1.127]	-287 ± 1 [1.126]	-257 ± 1 [1.126]	-197 ± 1 [1.125]	-200 ± 1 [1.125]	-179 ± 2 [1.125]
D_{24}	-117 ± 1 [1.031]	-108 ± 1 [1.031]	-96.8 ± 0.5 [1.031]	-74 ± 1 [1.031]	-75 ± 1 [1.031]	-67 ± 1 [1.031]
$D_{12'}$	-9 ± 1 [1.001]	-13 ± 1 [1.001]	-17 ± 1 [1.001]	-19 ± 1 [1.001]	-19 ± 1 [1.001]	-19 ± 1 [1.001]
D_{16}	-217 ± 1 [1.003]	-201 ± 1 [1.003]	-180 ± 1 [1.003]	-138 ± 2 [1.003]	-140 ± 1 [1.003]	-125 ± 2 [1.003]
D_{15}	-461 ± 3 [1.001]	-428 ± 3 [1.001]	-386 ± 2 [1.001]	-297 ± 4 [1.001]	-302 ± 3 [1.001]	-271 ± 5 [1.001]
D_{26}	-88.7 ± 0.4 [1.001]	-82 ± 1 [1.001]	-73.6 ± 0.3 [1.001]	-56 ± 1 [1.001]	-57 ± 1 [1.001]	-51 ± 1 [1.001]
D_{25}	-93 ± 8 [1.006]	-117 ± 7 [1.007]	-150 ± 8 [1.007]	-160 ± 6 [1.007]	-166 ± 6 [1.007]	-160 ± 8 [1.007]
D_{56}	-70 ± 1 [1.000]	-65 ± 1 [1.000]	-57.9 ± 0.5 [1.000]	-44 ± 1 [1.000]	-45 ± 1 [1.000]	-40 ± 3 [1.000]

Table S5: Simulated H-H solute dipolar couplings of selected hydrogen pairs (in Hz) for the case 2P/8CB. The ratios $\langle r_{ij}^{-3}\rangle/\langle r_{ij}\rangle^{-3}$ calculated from the simulations are given in square brackets. For the hydrogen labeling, see figure 1 in the main text.

	T = 294 K ($T_r = 0.963$)	T = 296 K ($T_r = 0.970$)	T = 298 K ($T_r = 0.977$)	T = 300 K ($T_r = 0.983$)	T = 302 K ($T_r = 0.990$)	T = 304 K ($T_r = 0.996$)
D_{12}	-3177 ± 9 [1.007]	-3094 ± 13 [1.007]	-3003 ± 15 [1.007]	-2891 ± 25 [1.007]	-2205 ± 23 [1.007]	-2055 ± 47 [1.007]
D_{13}	-924 ± 5 [1.926]	-895 ± 8 [1.925]	-867 ± 9 [1.924]	-833 ± 10 [1.923]	-623 ± 10 [1.918]	-578 ± 11 [1.916]
$D_{11'}$	164 ± 1 [1.001]	156 ± 2 [1.001]	150 ± 2 [1.001]	141 ± 3 [1.001]	99 ± 3 [1.001]	90 ± 4 [1.001]
$D_{22'}$	165 ± 1 [1.001]	157 ± 2 [1.001]	151 ± 2 [1.001]	142 ± 3 [1.001]	99 ± 3 [1.001]	90 ± 4 [1.001]
D_{14}	-272 ± 1 [1.126]	-264 ± 1 [1.126]	-257 ± 1 [1.126]	-248 ± 1 [1.126]	-189 ± 1 [1.125]	-176 ± 2 [1.125]
D_{24}	-102.1 ± 0.3 [1.031]	-99.4 ± 0.4 [1.031]	-96.6 ± 0.5 [1.031]	-93 ± 1 [1.031]	-71 ± 1 [1.031]	-66 ± 2 [1.031]
$D_{12'}$	-14 ± 1 [1.001]	-16 ± 1 [1.001]	-16 ± 1 [1.001]	-17 ± 1 [1.001]	-17 ± 1 [1.001]	-17 ± 1 [1.001]
D_{16}	-190 ± 1 [1.003]	-185 ± 1 [1.003]	-180 ± 1 [1.003]	-173 ± 1 [1.004]	-133 ± 1 [1.003]	-124 ± 3 [1.003]
D_{15}	-405 ± 1 [1.001]	-396 ± 2 [1.001]	-385 ± 3 [1.001]	-371 ± 3 [1.001]	-285 ± 3 [1.001]	-266 ± 6 [1.001]
D_{26}	-77.6 ± 0.2 [1.001]	-75.7 ± 0.3 [1.001]	-73.4 ± 0.4 [1.001]	-71 ± 1 [1.001]	-54 ± 1 [1.001]	-50 ± 1 [1.001]
D_{25}	-130 ± 6 [1.007]	-139 ± 6 [1.007]	-142 ± 7 [1.007]	-148 ± 6 [1.007]	-149 ± 6 [1.007]	-147 ± 5 [1.007]
D_{56}	-61.2 ± 0.3 [1.001]	-60 ± 1 [1.001]	-58 ± 1 [1.001]	-56 ± 1 [1.001]	-43 ± 1 [1.000]	-40 ± 3 [1.000]

Table S6: Average values of orientational order parameters $\langle P_2^{ij}\rangle$ and distances $\langle r_{ij}\rangle$ for the internuclear vector between protons i and j as obtained from simulations in the liquid crystal phase of 5CB.

T_r	$\langle P_2\rangle$ (12)	$\langle P_2\rangle$ (13)	$\langle P_2\rangle$ (11′)	$\langle P_2\rangle$ (22′)	$\langle P_2\rangle$ (14)	$\langle P_2\rangle$ (24)
0.942	0.44	0.081	-0.13	-0.13	0.27	0.35
0.959	0.41	0.076	-0.11	-0.11	0.25	0.33
0.975	0.36	0.070	-0.09	-0.09	0.23	0.29
0.992	0.28	0.056	-0.07	-0.07	0.18	0.23
0.995	0.28	0.056	-0.07	-0.07	0.18	0.23
0.998	0.25	0.051	-0.06	-0.06	0.16	0.21
$\langle r\rangle$ (Å)	2.45	3.37	4.31	4.28	5.18	7.33
T_r	$\langle P_2\rangle$ (12′)	$\langle P_2\rangle$ (16)	$\langle P_2\rangle$ (15)	$\langle P_2\rangle$ (26)	$\langle P_2\rangle$ (25)	$\langle P_2\rangle$ (56)
0.942	0.009	0.37	0.29	0.41	0.012	0.45
0.959	0.012	0.34	0.27	0.37	0.015	0.41
0.975	0.017	0.30	0.24	0.34	0.019	0.37
0.992	0.018	0.23	0.19	0.26	0.020	0.28
0.995	0.018	0.23	0.19	0.26	0.021	0.28
0.998	0.018	0.23	0.17	0.24	0.020	0.26
$\langle r\rangle$ (Å)	4.94	5.90	4.27	8.22	2.47	9.17

Table S7: Average values of orientational order parameters $\langle P_2^{ij}\rangle$ and distances $\langle r_{ij}\rangle$ for the internuclear vector between protons i and j as obtained from simulations in the liquid crystal phases of 8CB.

| T_r (phase)	$\langle P_2\rangle$(12)	$\langle P_2\rangle$(13)	$\langle P_2\rangle$(11′)	$\langle P_2\rangle$(22′)	$\langle P_2\rangle$(14)	$\langle P_2\rangle$(24)
0.963 (S)	0.38	0.073	-0.11	-0.11	0.25	0.31
0.970 (S)	0.37	0.071	-0.10	-0.10	0.24	0.30
0.977 (S)	0.36	0.069	-0.10	-0.10	0.23	0.29
0.983 (S)	0.35	0.067	-0.09	-0.09	0.22	0.28
0.990 (N)	0.26	0.053	-0.07	-0.07	0.17	0.21
0.996 (N)	0.25	0.050	-0.06	-0.06	0.16	0.20
$\langle r\rangle$ (Å)	2.45	3.33	4.30	4.28	5.18	7.33
T (K)	$\langle P_2\rangle$(12′)	$\langle P_2\rangle$(16)	$\langle P_2\rangle$(15)	$\langle P_2\rangle$(26)	$\langle P_2\rangle$(25)	$\langle P_2\rangle$(56)
0.963 (S)	0.014	0.32	0.26	0.35	0.016	0.39
0.970 (S)	0.016	0.31	0.25	0.34	0.018	0.38
0.977 (S)	0.016	0.30	0.25	0.33	0.018	0.37
0.983 (S)	0.017	0.29	0.24	0.32	0.019	0.35
0.990 (N)	0.017	0.22	0.18	0.24	0.019	0.27
0.996 (N)	0.017	0.21	0.17	0.23	0.019	0.25
$\langle r\rangle$ (Å)	4.94	5.90	4.27	8.22	2.47	9.17
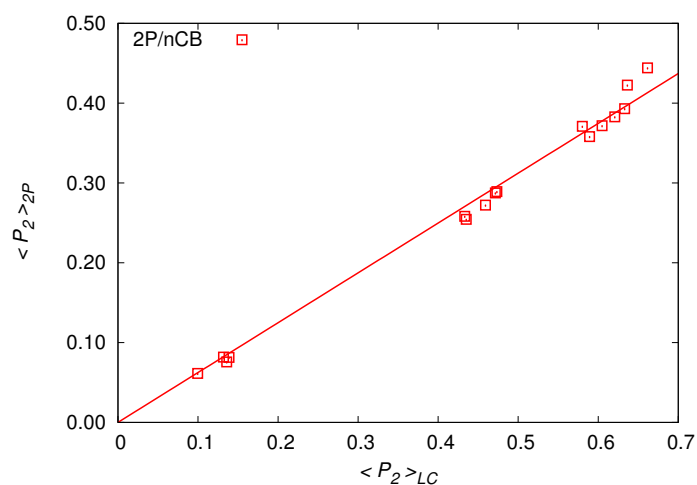
Figure S1: Orientational order parameters of 2P, $\langle P_2 \rangle_{2P}$, plotted against the corresponding $\langle P_2 \rangle_{LC}$ for both 5CB and 8CB solvent. The least square fitting line $\langle P_2 \rangle_{2P} = a\langle P_2 \rangle_{LC}$ is also plotted (a=0.645 ± 0.007, root mean square error 0.013). Partial outliers are the values of the order parameter in the 8CB phase.
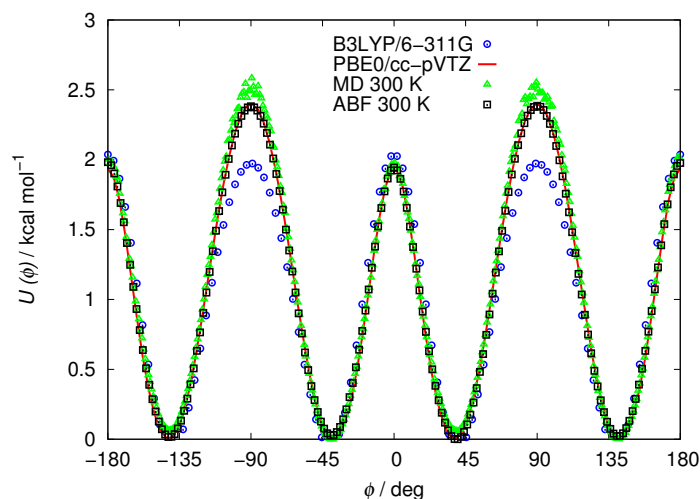

Figure S2: Torsional potential for biphenyl: B3LYP//6-311G(2d,p) (blue circles [49]); obtained in this work via BPE0//cc-pVTZ (red line); calculated from MD simulation in gas phase at 300 K assuming $U(\varphi) = -k_B T \ln P(\varphi)$ (green triangles) and using the adaptive biasing force method (black squares).
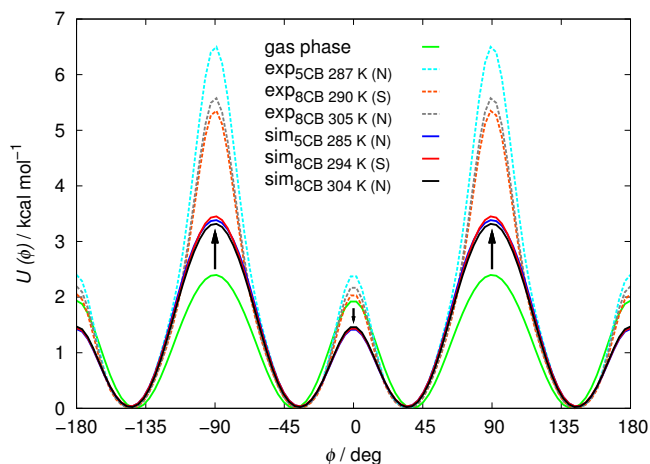
Figure S3: Torsional potential for 2P in LC obtained from experimental data with the AP method (cyan, orange and gray dashed lines) and via MD simulation (blue, red and black solid lines). The PBE0//cc-pVTZ potential is also reported (green line). Arrows indicate the changes induced by the LC solvent with respect to the vacuum as predicted by MD.

Positional order in the 8CB phase

The order parameters τ_1 and layer spacing d can be calculated following the procedure explained as method I in reference [27]. In practice, the positional order parameter is derived by scanning on a tentative layer spacing d' and the actual spacing d is the one that maximises τ_1, calculated as:

$$\tau_1(d') = \sqrt{\left[\left\langle \cos\left(\frac{2\pi z}{d'}\right)\right\rangle - \frac{d'}{2\pi L}\left\langle \sin\left(\frac{2\pi L}{d'}\right)\right\rangle\right]^2 + \left\langle \sin\left(\frac{2\pi z}{d'}\right)\right\rangle^2} \quad (8)$$

where the sampling is performed in a cylindrical region going from $-L$ to $+L$. and the corresponding values are reported in table S8.

Table S8: 8CB smectic order parameter τ_1 and layer spacing d.

T(K)	τ_1	d (Å)
294	0.14 ± 0.03	30.83 ± 0.83
296	0.14 ± 0.02	30.94 ± 0.85
298	0.14 ± 0.03	31.10 ± 0.74
300	0.13 ± 0.04	30.84 ± 1.33
302	0.06 ± 0.02	31.50 ± 3.36
304	0.05 ± 0.02	31.51 ± 3.43

Translational and rotational diffusion

We characterized the translational dynamics of the constituent molecules in MD simulation considering their diffusion coefficients:

$$D_\parallel = \lim_{\tau \to +\infty} \frac{\langle \Delta z^2(t) \rangle}{2\tau} \text{ and } D_\perp = \lim_{\tau \to +\infty} \frac{\langle \Delta x^2(t) \rangle}{2\tau} = \lim_{\tau \to +\infty} \frac{\langle \Delta y^2(t) \rangle}{2\tau} \qquad (9)$$

where $\langle \Delta z^2(t) \rangle$ is the mean square displacement of the particle along the director and $\langle \Delta x^2(t) \rangle$ and $\langle \Delta y^2(t) \rangle$ are the corresponding quantities perpendicular to the director. In simulations the infinite time limit cannot be reached but normally after some nanoseconds a linear regime of the square displacement is achieved [69]. Therefore, it is possible to extrapolate the diffusion coefficient from the slope of $\langle \Delta \mathbf{r}^2 \rangle$ versus time. As can be seen in figure S4 the diffusion along the director in the nematic phase is preferred both for solvent and solutes. At increasing temperature the parallel component of diffusion coefficients decreases and the perpendicular one assumes increasing values corresponding a decrease of $D_\parallel/D_\perp$ ratio until we reach the nematic–isotropic temperature transition, where the two components present the same value and $D_\parallel/D_\perp = 1$.

Regarding the rotational dynamics it can be expressed in terms of the decay time of the autocorrelation function of director cosines, i. e. $\langle \mathbf{x}(0) \cdot \mathbf{x}(t) \rangle$, $\langle \mathbf{y}(0) \cdot \mathbf{y}(t) \rangle$, $\langle \mathbf{z}(0) \cdot \mathbf{z}(t) \rangle$, where x, y, z are the molecular axes. For 2P, 5CB and 8CB, the z axis corresponds to the phenyl-phenyl para axis, the x axis is perpendicular to z and lies on a phenyl ring plane, while y is perpendicular to both x and z. The decay time (τ) is extrapolated by fitting with an exponential function $f(t) = e^{-\frac{t}{\tau}}$ where t is the simulation time and it assumes lower values along an axis if the molecule rotates faster in that direction. The description of the rotational velocity for biphenyl (tab. S9), for which a biaxial behavior with decay time maximum for the z axis is obtained and the orientational diffusion increases, as expected, with temperature while for nCB solvent instead the decay is mono-exponential. In particular the parallel diffusion with respect the director is greater then the perpendicular both for biphenyl and for nCB.
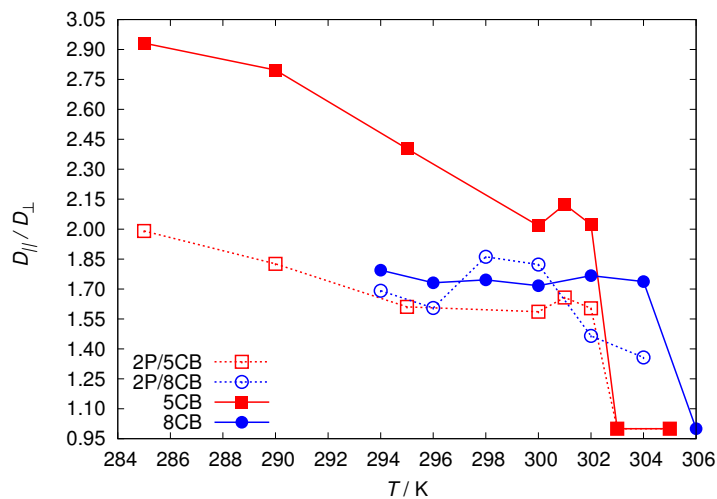
Figure S4: $D_\parallel/D_\perp$ ratio of 2P (empty points) both in 5CB (red) and 8CB (blue) solvent and for 5CB (filled red squares) and 8CB (filled red cyrcles) as function of temperature.

Table S9: Decay time (ns) of the autocorrelation function of director cosines for 2P/5CB and 2P/8CB.

	2P			5CB		
T(K)	τ_x	τ_y	τ_z	τ_x	τ_y	τ_z
285	0.071	0.121	0.215	0.086	0.086	14.932
290	0.060	0.104	0.171	0.073	0.073	8.876
295	0.052	0.090	0.137	0.063	0.063	5.453
300	0.045	0.077	0.105	0.057	0.057	2.381
301	0.044	0.075	0.104	0.056	0.056	2.330
	2P			8CB		
T(K)	τ_x	τ_y	τ_z	τ_x	τ_y	τ_z
294	0.045	0.078	0.118	0.066	0.066	8.993
296	0.042	0.074	0.112	0.062	0.062	7.878
298	0.039	0.069	0.105	0.058	0.058	6.395
300	0.038	0.066	0.097	0.055	0.055	5.208
302	0.036	0.062	0.085	0.051	0.051	2.271
304	0.033	0.057	0.078	0.047	0.047	2.139
306	0.032	0.053	0.069	0.045	0.045	1.052